

We are IntechOpen, the world's leading publisher of Open Access books Built by scientists, for scientists

6,000

Open access books available

148,000

International authors and editors

185M

Downloads

Our authors are among the

154

Countries delivered to

TOP 1%

most cited scientists

12.2%

Contributors from top 500 universities



WEB OF SCIENCE™

Selection of our books indexed in the Book Citation Index
in Web of Science™ Core Collection (BKCI)

Interested in publishing with us?
Contact book.department@intechopen.com

Numbers displayed above are based on latest data collected.
For more information visit www.intechopen.com



Low Energy Excitations in Borate Glass

Seiji Kojima

Abstract

The boson peak in the terahertz range is the low-energy excitations in glasses and disordered crystals. It is related to the excess part of the vibrational density of states. Borate glass is one of the typical network oxide glasses with covalent bonds and belongs to the strong type of glass formers. Alkali metal ions are well-known modifiers of the borate glass network and control various properties. The alkali metal effects are reviewed on basic physical properties such as elastic constants, density, and vibration modes in relation to the variation of structural units in a modified borate glass network. The alkali effect on a boson peak is discussed on the basis of experimental results of neutron inelastic scattering, neutron diffraction, Raman scattering, and heat capacity at low temperatures. The correlation is discussed between the boson peak frequency, the peak temperature of excess heat capacity, and shear modulus. The static and dynamical correlation lengths are also discussed.

Keywords: borate glass, boson peak, FSDP, medium range order, fragility, relaxation, excess heat capacity

1. Introduction

2022 is declared a United Nations International Year of Glass (IYOG), which celebrates the heritage and importance of this material in our lives [1]. Glass is technologically very important in industry, and it is clear that modern life would not be possible without glass. Glass is also very interesting in fundamental sciences related to random structure and non-equilibrium state. When a viscous liquid is cooled from a high temperature, it changes into a supercooled liquid state, and upon further cooling, it undergoes a liquid–glass transition into a nonequilibrium glassy state at a glass transition temperature T_g . However, a simple liquid is solidified into an equilibrium crystalline state at its melting temperature, T_m . The temperature dependence of enthalpy is shown in **Figure 1** for a liquid (AB), supercooled liquid (BD), glassy (DE), and crystalline (CG) states. The enthalpy of a liquid crosses to that of a crystal at the point, F, which is the Kauzmann temperature, T_K [1]. It is a static ideal glass transition temperature and close to the Vogel–Fulcher temperature, the dynamic ideal glass transition temperature, T_{VF} [3, 4], which is lower than the calorimetric T_g .

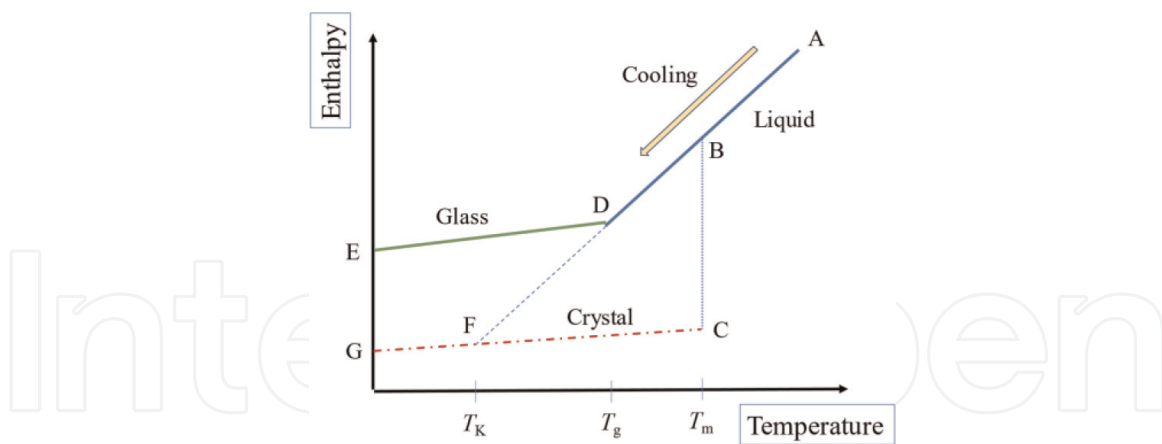


Figure 1.

Temperature dependence of the enthalpy for the liquid (AB), supercooled liquid (BD), glass (DE), and crystalline (CG) states, where T_m , T_g , and T_K are the melting, glass transition, and Kauzmann temperatures, respectively [2].

The temperature dependence of the relaxation time, τ_α , of α -structural relaxation process obeys the following Vogel-Fulcher law and the relaxation time diverges at T_{VF} .

$$\tau_\alpha = \tau_0 \exp\left(\frac{B}{T - T_{VF}}\right) \text{ for } T > T_{VF} \quad (1)$$

Here, τ_0 and B are material-dependent constants, and $T_g > T_{VF}$. The fragility index m is defined by Eq. (2) using the parameters of Eq. (1). When the intermolecular interactions are weak, m is large and materials are fragile. While the interactions are strong, Eq. (1) goes to the Arrhenius law and materials are strong.

$$m = \left[\frac{d \log \tau_\alpha}{d \left(\frac{T_g}{T} \right)} \right]_{T=T_g} = \frac{B}{T_g \ln 10 (1 - T_{VF}/T_g)^2} \quad (2)$$

In a liquid-glass transition, main three dynamical processes are the α -structural relaxation, fast β -relaxation, and boson peak. These three dynamics are interrelated with each other. According to the mode-coupling theory, the α -relaxation is related to the creation and annihilation of a molecular cage, the fast β -relaxation is related to a relaxation of molecules trapped in their cages. A boson peak is related to a damped librational motion of molecules trapped in their cages [5].

Glycerol (propane-1,2,3-triol, $C_3H_8O_3$) undergoes a liquid-glass transition at about $T_g = 187$ K. Glycerol is intermediate with $m = 53$. The melting temperature is $T_m = 291$ K, while it does not crystallize even in very slow cooling. It is one of the typical glass-forming materials and well-known cryoprotectants due to its strong glass-forming tendency [6]. The dominant interaction among molecules is the intermolecular hydrogen bond, and the related O-H stretching band showed a remarkable temperature dependence in the vicinity of T_g [7]. By the broadband dielectric spectroscopy, the slowing down of the α -relaxation time towards T_g , which obeys the Vogel-Fulcher law of Eq. (1), was clearly observed in the milli hertz to gigahertz range [8]. For the dynamical properties in the terahertz range, the temperature dependence of low-frequency Raman scattering spectra is shown in **Figure 2** [9]. The remarkable changes in Raman spectra were observed in the low-frequency range. In a liquid phase at 328

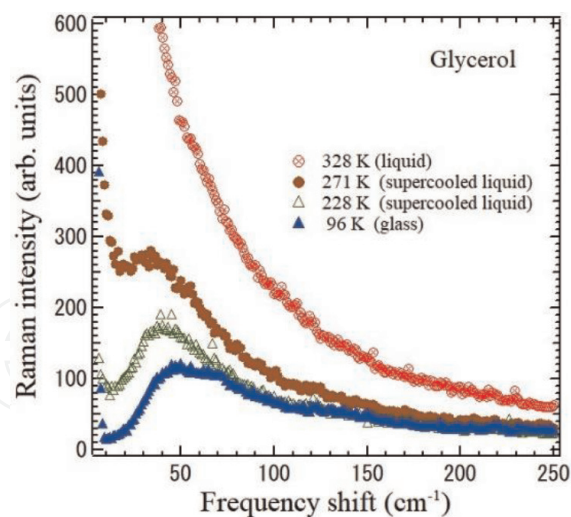


Figure 2.
Temperature dependence of low-frequency Raman scattering spectra of a liquid-glass transition of glycerol [9].

K, the broad Rayleigh wing appears, and the main contribution of this wing is the α -structural relaxation and fast β -relaxation. In supercooled liquid states at 271 and 228 K, the α -relaxation time becomes slow and the contribution to the Rayleigh wing becomes small. While the fast β -relaxation time does not depend on temperature, and its intensity gradually changes into a boson peak at about 40 cm^{-1} ($=1.2 \text{ THz}$). In a glass state at 96 K, only a boson peak appears. The liquid-phase transition also occurs by the application of hydrostatic pressure at room temperature at $P_g = 5 \text{ GPa}$. The boson peak was also observed in the pressure-induced glass state [10]. These dynamical properties on the boson peak, α - and fast β -relaxation processes in **Figure 1** are common in liquid-glass transitions of organic and inorganic glass-forming materials.

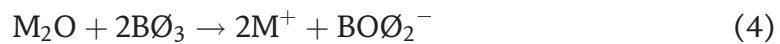
2. Borate glass and alkali metal modification

Borate glass is the most contemporary glass and optical material for technological and environmental applications. Pure borate glass undergoes a glass transition at $T_g = 260^\circ\text{C}$. The melting temperature is $T_m = 450^\circ\text{C}$ [11]. The character of the temperature dependence of thermal expansibility, surface tension, and viscosity, in the range up to 1400°C , proves that, in the crystalline state and in the vitreous state below about 300°C , boron oxide consists of units held together by “weak” forces and that with increasing temperature this structure changes gradually toward a “strong” one [10]. The borate glass is strong with a fragility index of $m = 30$. Boron oxide glass has a random three-dimensional network of BO_3 -triangles with a comparatively high fraction of six-membered rings (boroxol rings). Krogh-Moe discussed structure models for boron oxide glass and molten boron oxide with reference to spectroscopic data, diffraction data, and other physical properties for boron oxide [12]. Borate glasses for scientific and industrial applications were reviewed by Bengisu [13].

Borate glass is modified by alkali metals and physical properties remarkably change by the appearance of various structural units and structural groups. In this chapter, we discuss the dynamical properties of binary alkali metal borate glasses, $x\text{M}_2\text{O}(1-x)\text{B}_2\text{O}_3$ ($\text{M} = \text{Li}, \text{Na}, \text{K}, \text{Rb}, \text{Cs}$), i.e., lithium borate (LiB), sodium borate (NaB), potassium borate (KB), rubidium borate (RbB), and cesium borate (CsB) glasses. In alkali borate glasses, the physical properties are of special interest, because

their alkali content dependences often show maxima and minima termed “borate anomaly” [14]. Their dependence also shows the difference among the kind of alkali metal ions. The dependences of density against the alkali content are classified to two groups. In LiB, NaB, and KB glasses, density shows a moderate increase as the alkali content increases, and they have the nature of covalent packing. While in RbB and CsB glasses, density remarkably increases against the alkali content increases, and they have the nature of ionic packing [15].

Since the physical properties are related to the structure, the variation has been discussed in terms of three kinds of structural units, $B\emptyset_3$, $B\emptyset_4^-$, and $BO\emptyset_2^-$, for the alkali content below $x = 0.50$ as shown in **Figure 3** [15, 16]. Here, O and \emptyset denote the nonbridging and bridging oxygens, respectively. In pure borate glass, the coordination number of boron is three, and units $B\emptyset_3$ are dominant. When borate glass is modified by alkali ions, the units $B\emptyset_4^-$ and $BO\emptyset_2^-$ are formed by the chemical reactions of Eqs. (3) and (4). The two units coexist by the disproportionation reactions of Eq. (5). As the ionic radius of alkali ions increases, the number of nonbridging oxygen increases and the average coordination number of boron decreases. Consequently, the number of $B\emptyset_4^-$ decreases, while that of $BO\emptyset_2^-$ increases.



For the detailed discussion on the variation of structure, several kinds of super-structural units or structural groups such as boroxol ring, pentaborate, and diborate groups were considered [17].

For the analysis on the variation of physical properties, we introduce the quantity $V_m(B)$ and $V_m(O)$, which denote the volume of glass containing one a mole of boron and oxygen, respectively.

$$V_m(B) = \frac{M[xM_2O(1-x)B_2O_3]}{2\rho(1-x)} \quad (6)$$

$$V_m(O) = \frac{M[xM_2O(1-x)B_2O_3]}{\rho(3-2x)} \quad (7)$$

Where ρ is density, $M[xM_2O(1-x)B_2O_3]$ is the molar mass of the entity $xM_2O(1-x)B_2O_3$. **Figure 4** shows alkali content dependences of volumes of glass containing one mole of (a) boron and (b) oxygen atoms [15].

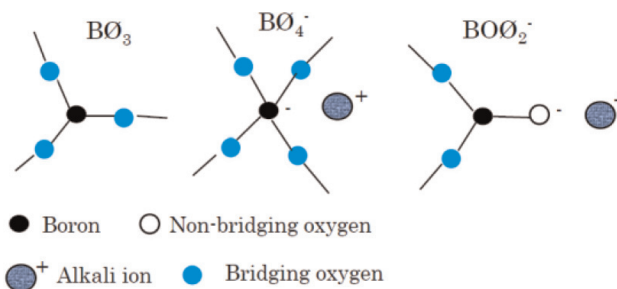


Figure 3.
Structural units of alkali borate glasses.

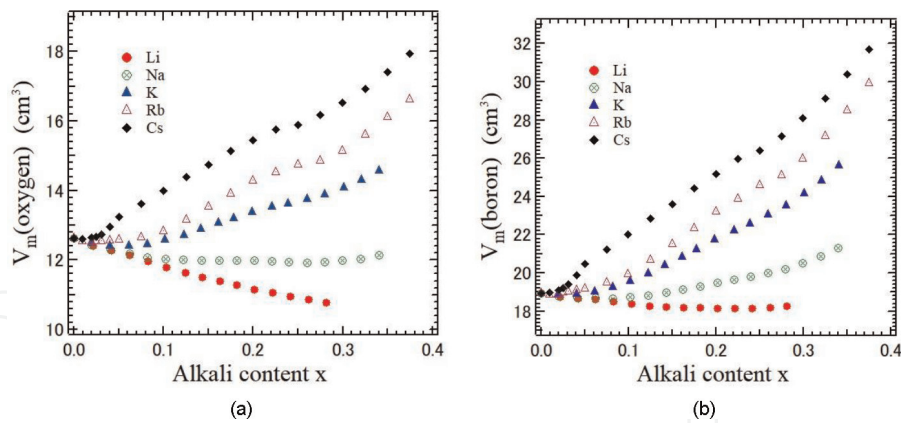


Figure 4. Alkali content dependences of volumes of glass containing one mole of (a) boron, and (b) oxygen atoms.

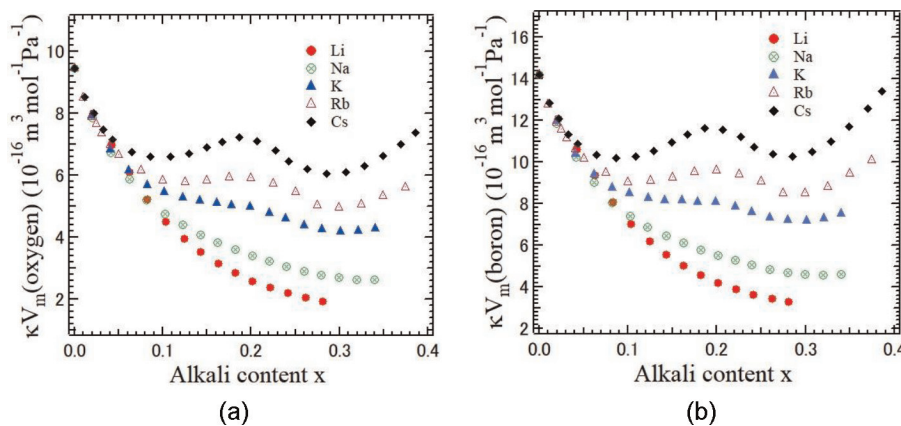


Figure 5. Alkali content dependences of the derivatives of the molar volumes (a) $\kappa V_m(B)$, and (b) $\kappa V_m(O)$ of alkali borate glasses [15].

Both $V_m(B)$ and $V_m(O)$ increase with respect to alkali content in LiB, NaB, and KB glasses, while they decrease in RbB and CsB glasses. At a given alkali content, the packing of boron and oxygen in the glass structure becomes more compact as the ionic radius of alkali ion increases. The boron atoms are packed most compactly at $x = 0.20$ for LiB, $x = 0.08$ for NaB, $x = 0.02$ for KB, $x = 0.01$ for RbB, and none for CsB glasses.

The remarkable changes occur in the response to the stress such as their pressure derivatives. We discuss the derivatives of the molar volumes $V_m(B)$ and $V_m(O)$ with respect to pressure.

$$-\frac{d}{dp} V_m(B) = -\frac{1}{V} \frac{dV}{dP} V_m(B) = \kappa V_m(B), \quad (8)$$

$$-\frac{d}{dp} V_m(O) = -\frac{1}{V} \frac{dV}{dP} V_m(O) = \kappa V_m(O), \quad (9)$$

where $\kappa = -\frac{1}{V} \frac{dV}{dP}$, is the compressibility. The $\kappa V_m(B)$ represents the effect of boron atoms on the elasticity, and the $\kappa V_m(O)$ represents the effect of oxygen atoms on the elasticity. **Figure 5** shows the alkali content dependences of $\kappa V_m(B)$ and $\kappa V_m(O)$ [15].

Both $\kappa V_m(B)$ and $\kappa V_m(O)$ at a given alkali content decrease as the ionic radius of alkali ions increases. In LiB and NaB glasses with covalent packing, $\kappa V_m(B)$ and $\kappa V_m(O)$ monotonically decrease. However, in KB, RbB, and CsB glasses with ionic packing, the concave and convex shapes appear. We discuss these dependences by the division into following three alkali content ranges.

- $0 \leq x \leq 0.07$: The conversion of $B\emptyset_3 \rightarrow B\emptyset_4^-$ in Eq. (3) is dominant and $\kappa V_m(B)$ and $\kappa V_m(O)$ decrease. The glass becomes incompressible with no alkali dependence.
- $0.07 \leq x \leq 0.2$: The conversion of $B\emptyset_3 \rightarrow B\emptyset_4^-$ continues. However, in RbB and CsB glasses, the formation of $B\emptyset_3 \rightarrow BO\emptyset_2^-$ in Eq. (4) also occurs. The $\kappa V_m(B)$ and $\kappa V_m(O)$ increase by the presence of the small amount of $M^+ BO\emptyset_2^-$ units. At a given alkali content, this conversion decreases as the ionic radius of alkali ion decreases.
- $0.2 \leq x \leq 0.3$: The conversion of $B\emptyset_3 \rightarrow B\emptyset_4^-$ does not occur. The volume of $M^+ BO\emptyset_2^-$ unit is larger than that of $M^+ B\emptyset_4^-$ unit and easily deformed by stress. Thus, the increase of small amount of $M^+ BO\emptyset_2^-$ units causes the glass incompressible, and at $x = 0.3$ RbB and CsB glasses have the most compact structure.
- $0.3 \leq x \leq 0.4$: By the formation of the large amount of $M^+ BO\emptyset_2^-$ units, the glass becomes more compressible and elastically softer.

3. Elastic properties of alkali borate glasses

Since the low-energy excitations in glass is closely related to the acoustic modes, the sound velocity was measured by the ultrasonic pulse-echo overlap method at a frequency of 10 MHz and at 298 K [15, 16]. The sound velocities of longitudinal acoustic (LA) and transverse acoustic (TA) modes of the binary alkali metal borate glasses, $xM_2O(1-x)B_2O_3$ ($M = Li, Na, K, Rb, Cs$) are shown in **Figure 6a** and **b**,

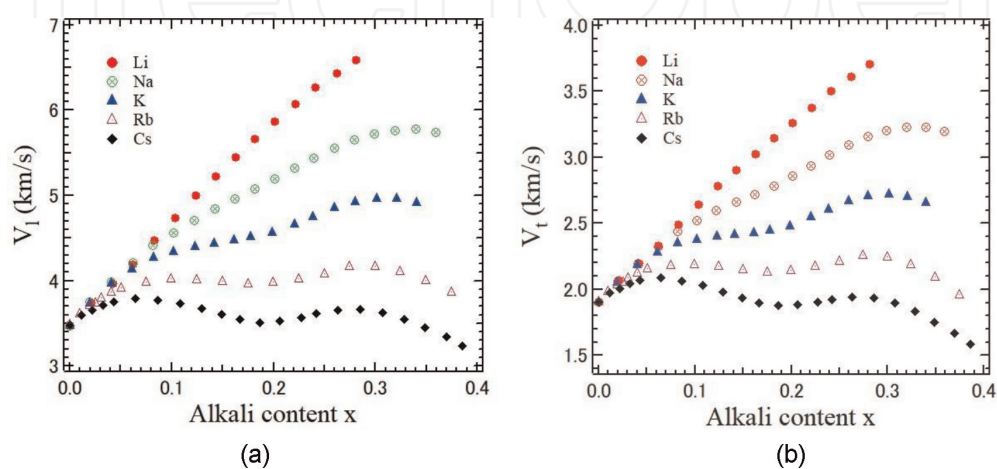


Figure 6. Alkali content dependences of velocity of (a) longitudinal, and (b) transverse acoustic modes.

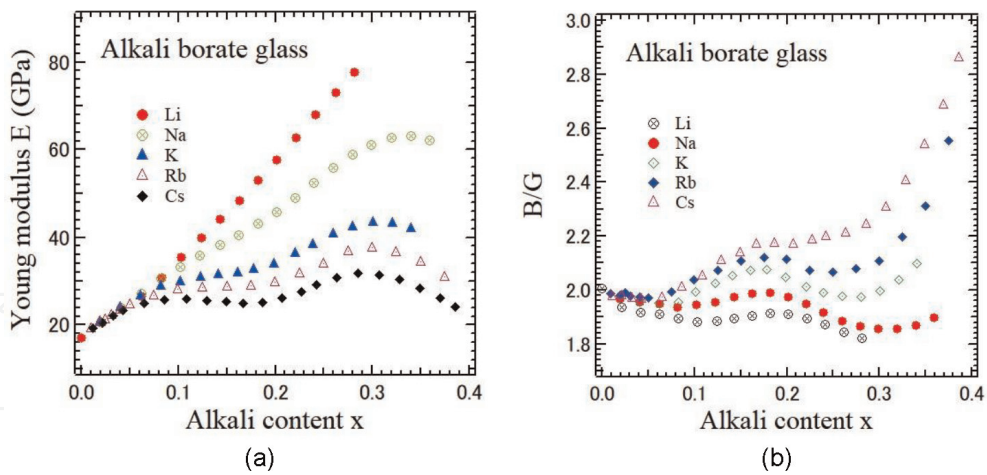


Figure 7. Alkali content dependences of (a) Young's modulus, E , and (b) the ratio between bulk and shear moduli, B/G .

respectively [17]. These dependences have a similarity with those of the reciprocal plots of $\kappa V_m(B)$ and (b) $\kappa V_m(O)$ in **Figure 5a** and **b** reflecting the variation of structural units by alkali ions.

Using the LA and TA velocities, the following elastic moduli were calculated.

$$\text{Shear modulus : } G = \rho V_T^2 \quad (10)$$

$$\text{Longitudinal modulus : } L = \rho V_L^2 \quad (11)$$

$$\text{Poisson's ratio : } \sigma = \frac{1}{2} \frac{V_L^2 - 2V_T^2}{V_L^2 - V_T^2} \quad (12)$$

$$\text{Young's modulus : } E = 2G(1 + \sigma) \quad (13)$$

$$\text{Bulk modulus : } B = L - \frac{4}{3}G \quad (14)$$

$$\text{Compressibility : } \kappa = 1/B \quad (15)$$

Figure 7a shows the alkali content dependences of Young's modulus. In the Young's modulus of LiB and KB glasses, the monotonic increase was observed. However, in that of KB, RbB, and CsB glasses concave and convex shapes were observed. Such alkali dependence of Young's modulus is similar to that of $\kappa V_m(B)$ in **Figure 5a**.

The plot of bulk versus shear moduli is helpful in distinguishing ductile from brittle behavior beyond the elastic limit. When $B/G \gg 1$ ($\sigma = 0.5$), materials are extremely incompressible. For ceramics, $B/G \approx 1.7$ ($\sigma \approx 0.25$). For polymers, $B/G \approx 2.7$ ($\sigma \approx 0.33$). When $B/G \ll 1$ ($\sigma = -1$), materials are extremely compressible. The B/G is also related to the boson peak intensity and the fragility index [18]. The ratio between bulk and shear modulus is plotted in **Figure 7b**. The B/G is between 1.8 and 2.9. The B/G shows the concave and convex shapes were observed in all the alkali borate glasses. These dependences are explained by the division of four alkali content ranges. (a) $0 \leq x \leq 0.07$: The $B\text{O}_3$ changes into $B\text{O}_4^-$ only and does not change into BOO_2^- . (b) $0.07 \leq x \leq 0.20$: The $B\text{O}_3$ changes into both $B\text{O}_4^-$ and BOO_2^- . The effect of BOO_2^- is predominant over that of $B\text{O}_4^-$. (c) $0.20 \leq x \leq 0.30$: The $B\text{O}_3$ changes into both $B\text{O}_4^-$ and BOO_2^- . The effect of $B\text{O}_4^-$ is predominant over that of BOO_2^- . (d) $0.30 \leq x \leq 0.40$: The $B\text{O}_3$ changes only into BOO_2^- without the further formation of $B\text{O}_4^-$.

4. Boson peaks of alkali borate glasses

In glasses the universal features of their thermal properties at low temperatures have been observed. The heat capacity shows an excess part as the deviation from the Debye T^3 law and the thermal conductivity has a plateau at around 10 K [19]. These universal behaviors are caused by the anomalous phonon dispersion in the terahertz frequency (THz) range. In the inelastic scattering spectra, the peak of $g(E)/E^2$ has been observed, where $g(E)$ and $E=h\nu$ are the vibrational density of states (VDoS) and energy, respectively. The origin of a peak is the low-energy excess part of VDoS over the Debye model defined by $g(E)/E^2$. This THz peak is called the boson peak [20]. In the measurement of heat capacity C_p at low temperatures, a bump in C_p/T^3 at around 10 K is called a thermal boson peak. The plateau of the thermal conductivity indicates the strongly scattered of phonons above the boson peak frequency. It indicates that phonons meet the transverse Ioffe–Regel (IR) limit [21] around the boson peak.

The microscopic origin of a boson peak has been discussed by various theoretical models, such as (1) the structure and elastic constants heterogeneity [22–24]; (2) soft potential model [24–26]; (3) the resonant vibration of medium range order [27]; (4) mode-coupling theory on density fluctuations of arrested glass structures [28]; (5) broadening of the lowest van Hove singularity of the transverse phonon branch [29]; (6) the phonon-saddle transition in the energy landscape [30]; (7) the random first-order transition theory (RFOT) [31]; (8) anharmonic effects [32], and (9) recent numerical calculations reported that the boson peak originates from quasi-localized vibrations of string-like dynamical defects [33]. However, this situation has remained quite controversial because of a lack of distinct evidence.

The Stokes-component of Raman scattering intensity $I(\nu)$ is related to the imaginary part of Raman susceptibility $\chi''(\nu)$.

$$I(\nu) = I_0 \chi''(\nu) \{n(\nu) + 1\}, \quad n(\nu) = \frac{1}{\exp\left(\frac{h\nu}{k_B T}\right) - 1} \quad (16)$$

where $n(\nu)$ is the Bose-Einstein factor and I_0 is a constant which depends on the experimental condition. For the discussion of the boson peak in a Raman spectrum, the following quantity is plotted. Here, $C(\nu) = \nu^\alpha$ ($\alpha=0\sim 2$) is the light-vibration coupling constant and its frequency dependence shows a monotonic increase [20].

$$\frac{\chi''(\nu)}{\nu} = \frac{I(\nu)}{\nu \{n(\nu) + 1\}} \propto C(\nu) \frac{g(\nu)}{\nu^2} \quad (17)$$

Figure 8a shows the boson peak spectra of lithium borate glasses observed by Raman scattering using a triple-grating spectrometer with the additive dispersion. The boson peak frequency $\nu_{BP} = 26 \text{ cm}^{-1}$ at $x = 0.02$ increases up to 72 cm^{-1} at $x = 0.26$ as the lithium content increases and the increase is related to the increase of transverse sound velocity shown in **Figure 5b** [34]. In LiB glasses, the fragility index m increases from 30 at $x=0.00$ to 62 at $x=0.28$. In strong glass, the boson peak intensity is high, while the intensity of the fast β -relaxation is weak. As the fragility index m increases, the boson peak intensity becomes weak and that of the fast β -relaxation increases. As shown in **Figure 8a** the boson peak intensity decreases as the Li content increases.

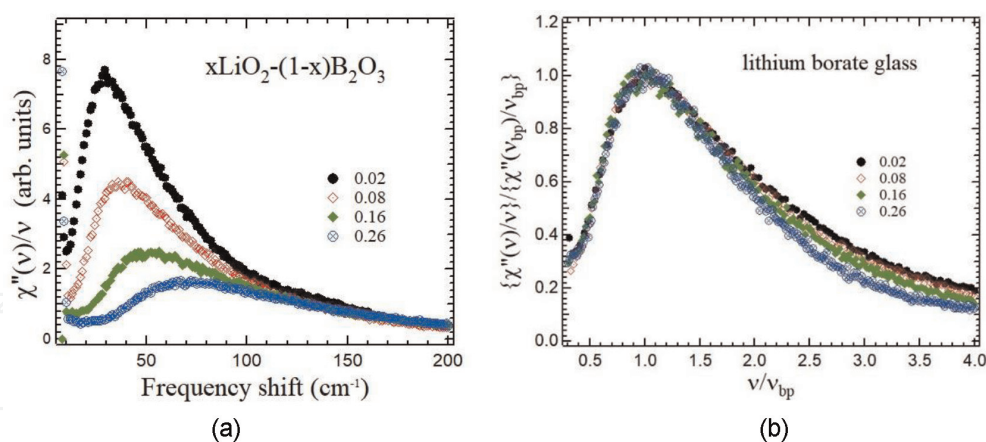


Figure 8. (a) Reduced Raman spectra of boson peaks of lithium borate glasses observed by Raman scattering, and (b) Scaled boson peak spectra.

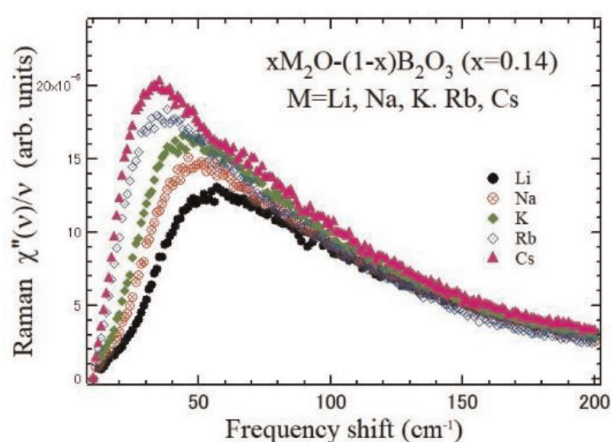


Figure 9. Reduced Raman spectra of boson peaks of alkali borate glasses ($x=0.14$).

It is interesting to check that the boson peak spectra of inelastic neutron scattering, and Raman scattering are scaled by their peak positions and scattering intensity. In LiB glasses, it is found that the scaled boson peak spectra have a universal shape as shown in **Figure 8b**. The universal scaling of boson peaks indicates that the way of the distribution of VDoS basically remains the same, even though the glass structures drastically change by the alkali metal modification.

The alkali dependence of boson peak spectra at $x=0.14$ is shown in **Figure 9**. The origin of the boson peak in a pure borate glass was attributed to the coherent libration of several boroxol rings based on the study of the hyper-Raman scattering. As the alkali content increases, these boroxol rings change into other boron-oxygen structural units. As the ionic radius of alkali ions increases, the boson peak frequency decreases reflecting the difference in the modification of glass structure by alkali ions. Since the large Cs ions with the low charge density only slightly changes the boron-oxygen network structure. However, the small Li ions with the high charge density cause shrinking of the boron-oxygen network structure [35, 36]. By application of high pressure, it was reported that the boson peak frequency significantly increases up to 68 cm^{-1} at 4 GPa by shrinking of the boron-oxygen network structure [37]. The alkali content dependence of boson peaks of LiB glasses has the similarity with the densified borate glasses.

The boson peak frequency in a Raman spectrum includes the influence of the light-vibration coupling constant $C(\nu)$ as shown in Eq. (17). However, the boson peak in a neutron inelastic spectrum enables the direct observation of a boson peak frequency or energy even in the S/N ratio of scattering intensity is much lower than that of Raman scattering. **Figure 10** shows the alkali dependence of boson peak spectra of alkali borate glasses at $x=0.22$ observed by cold neutron inelastic scattering. Neutron inelastic scattering measurements of all the alkali borate glasses were carried out at 25° C (far below the T_g) using a direct geometry chopper-type ToF spectrometer AGNES belonging to the Institute for Solid State Physics, University of Tokyo [38]. The neutron boson peak energy also decreases as the ionic radius of alkali ions increases. As the charge density decreases with the increase in ionic radius, the contraction of the boron–oxygen structural units become weaker and the boson peak energy may decrease.

If we assume that the boson peak is connected to the nano-heterogeneity of the shear modulus [27]. In this approach, a dynamic length scale, L_{BP} , is given by

$$L_{BP} = V_t / 2\pi\nu_{BP}, \quad (18)$$

where V_t is the transverse sound velocity, and ν_{BP} is the boson peak frequency. The L_{BP} corresponds to a medium-range scale important for characterization of structure

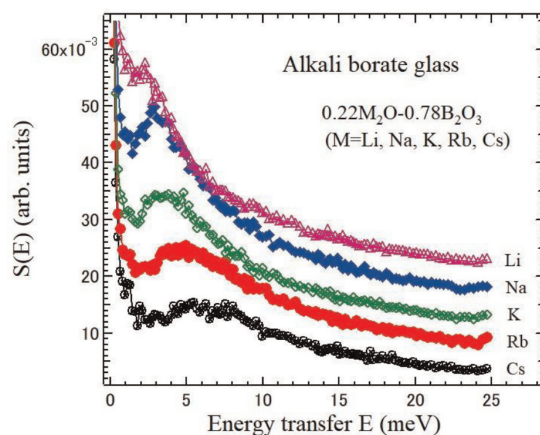


Figure 10. Boson peaks of alkali borate glasses at $x=0.22$ observed by cold neutron inelastic scattering [37].

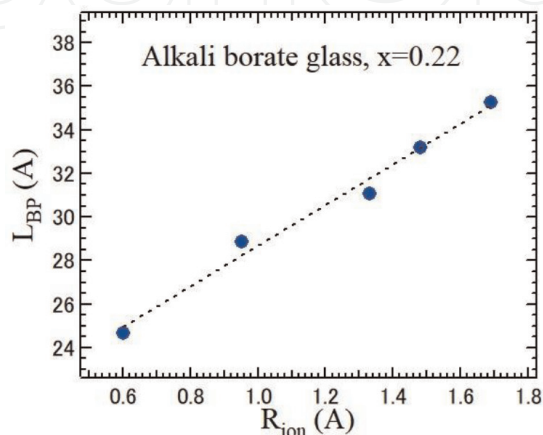


Figure 11. The correlation between L_{BP} and ionic radius of alkali ions in alkali borate glasses.

correlations in glasses. The good correlation between L_{BP} and ionic radius of alkali ions is found as shown in **Figure 11**. It is found that L_{BP} is proportional to the ionic radius of alkali ions. It indicates that the dynamic length of a boson peak may relate to the size of alkali ion in the void of boron-oxygen network structure.

5. Excess heat capacity at low temperatures of alkali borate glasses

The excess heat capacity has been observed as the deviation from the Debye T^3 law at low temperatures. The broad peak in a C_p/T^3 vs. T plot is the thermal boson peak, where C_p is the heat capacity at a constant pressure. It is related to the non-Debye excess heat capacity. The alkali content dependence of C_p/T^3 in lithium borate glasses is shown in **Figure 12** [35]. In the pure borate glass, the peak of C_p/T^3 was observed at the temperature, $T_m = 5.8$ K [39]. As the lithium content increases, the peak value decreases and the peak temperature increases. Such a behavior of the peak value and the peak temperature of thermal boson peaks is similar to the peak intensity and peak frequency of boson peaks observed by Raman scattering and neutron inelastic scattering, respectively.

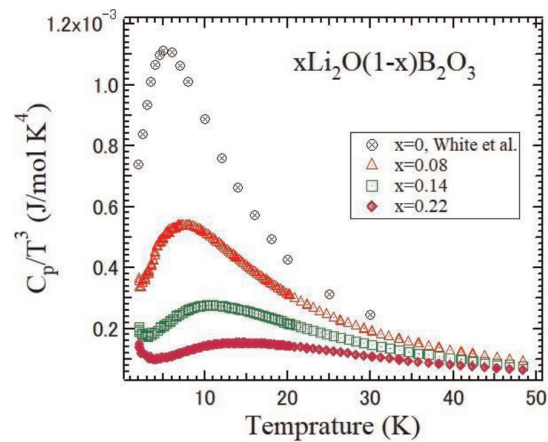


Figure 12.
 Temperature dependence of C_p/T^3 of lithium borate glasses at low temperatures.

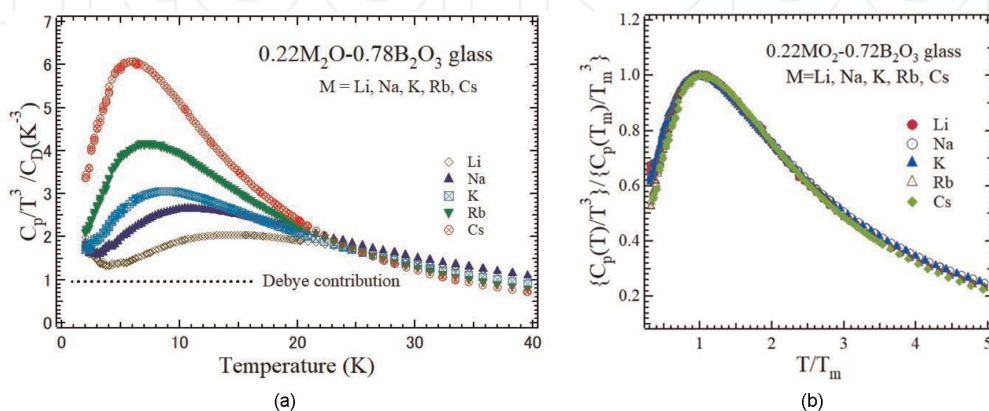


Figure 13.
 (a) Temperature dependence of C_p/T^3 of alkali borate glasses normalized by Debye contribution at low temperatures, and (b) Scaled thermal boson peaks of alkali borate glasses.

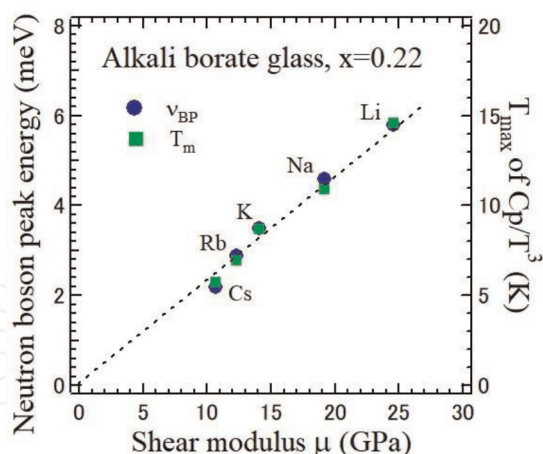


Figure 14. Correlation between the peak temperature of C_p/T^3 , boson peak frequency, and shear modulus.

The temperature dependence of C_p/T^3 of alkali borate glasses with $x=0.22$ below 50 K is shown in **Figure 13** [35]. The peak temperature of CsB glass is close to that of pure borate glass. However, as the ionic radius of alkali metal ions decreases, the peak temperature markedly increases. The peak temperature of LiB glass is $T_m=14.6$ K, which is about three times of a pure borate glass.

For all the alkali borate glasses, the universal nature of the master plot in C_p/T^3 vs. T is also observed as shown in **Figure 13b**. This universal nature is the same as that of boson peaks observed by Raman scattering and neutron inelastic scattering. This fact indicates that the distribution of the low-energy excess VDoS remains the same for all the alkali modification.

On the discussion on the origin of a boson peak, the correlation between the transverse acoustic mode and a boson peak is very interesting. According to the numerical simulation, the equality of the boson peak frequency to the Ioffe–Regel limit for “transverse” phonons was reported. The boson peak energy is proportional to the shear modulus [40]. Since the peak temperature of a thermal boson peak is proportional to the boson peak frequency, the correlation is examined between the peak temperature of C_p/T^3 , boson peak energy, and shear modulus. The good correlation is found between these quantities as shown in **Figure 14**. This fact indicates that the origin of a boson peak is closely related to the Ioffe-Regal limit for transverse acoustic waves.

6. Medium range order of alkali borate glasses

In contrast to crystals with translational symmetry, glasses have disordered structure about local atomic arrangements. However, the structure of glasses has the medium range order (MRO) on a few nanometers’ length scale [41, 42]. The MRO in liquid and glassy states is characterized by the first sharp diffraction peak (FSDP). The FSDP is observed by neutron and X-ray diffraction experiments in the static structure factor $S(Q)$, where Q is the modulus of the wave vector [43]. The peak position Q_1 and the peak width ΔQ of a FSDP correspond to a periodic ordering with a periodicity of $2\pi/Q_1$ and a static structure correlation length L_{fsdp} given by

$$L_{\text{fsdp}} = 2\pi/\Delta Q \quad (19)$$

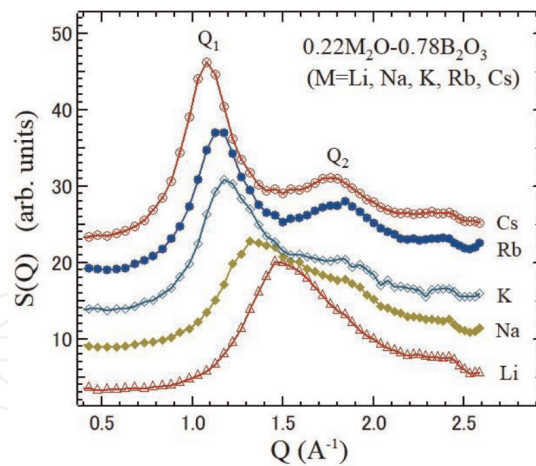


Figure 15. Static structure factor $S(Q)$ of alkali borate glasses observed by neutron diffraction. Q_1 is the position of a FSDP.

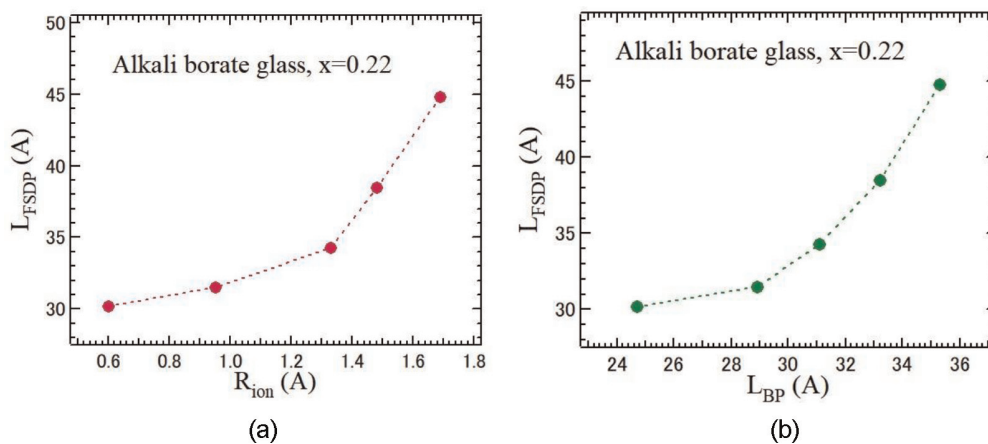


Figure 16. (a) Correlation between the static structure correlation length of FSDP and the ionic radius of alkali ions of alkali borate glasses, and (b) Correlation between the static structure correlation lengths of a FSDP and the dynamic correlation length of a boson peak.

respectively. It was reported that the FSDP intensity and peak position can be quantified using the characteristic void distribution function, defined in terms of average void size, void distance, and void density [44].

The static structure factor $S(Q)$ of alkali borate glasses determined by the neutron scattering is shown in **Figure 15** [38]. As the ionic radius of alkali ions decreases, the position Q_1 of a FSDP increases. Using the peak width of a FSDP, the static structure correlation lengths L_{fsdp} are determined. The correlation between the static structure correlation length and ionic radius of alkali ions is plotted in **Figure 16a**. It is found that as the ionic radius increases, the correlation length also increases. The MRO may be related to the local structure in the vicinity of an alkali ion in voids.

The correlation of various glasses between the boson peak frequency and the width of a FSDP was reported by Sokolov et al. [45]. Since the boson peak frequency is related to the dynamical correlation length L_{BP} , the relation between the static structure correlation length and the dynamical correlation length is plotted in **Figure 16b**. The good correlation between the dynamical correlation length L_{BP} and the static structure correlation length L_{fsdp} indicates that the boson peak is the vibration related to the MRO defined by the width of a FSDP.

7. Conclusions

Borate glass is most contemporary glasses and optical materials for technological and environmental applications. Borate glass is one of the typical network oxide glasses with covalent bonds and belongs to the strong type of glass formers. Alkali metal ions are well known modifiers of the borate glass network and control various properties. Basic physical properties such as elastic constants, density, and vibration modes are reviewed in relation with the variation of structural units in modified borate glass network.

The boson peak in the terahertz range is the low-energy excitations in glasses and disordered crystals. It is related to the excess part of vibrational density of states. The alkali metal effects on the boson peak are discussed on the basis of experimental results of neutron inelastic scattering, neutron diffraction, Raman scattering, low-temperature heat capacity, and ultrasonic measurements. For all the alkali borate glasses, the universal nature of the master plots in boson peak spectra and C_p/T^3 vs. T curve are observed. This fact indicates that the distribution of the low-energy excess VDoS remains the same for all the alkali modification.

The good correlation is found between the peak temperature of C_p/T^3 , boson peak frequency, and shear modulus. This fact indicates that the origin of a boson peak is closely related to the Ioffe-Regal limit for transverse acoustic waves. The static and dynamical correlation lengths show also the good correlation. As the ionic radius of alkali ions increase, both correlation lengths also increase. This fact suggests that the boson peak vibration is related to the medium range order in the boron-oxygen network near the voids filled by alkali ions.

Acknowledgements


The author is thankful to Prof. M. Kodama, Prof. S. A. Feller, Prof. M. Affatigato, Prof. V. N. Novikov, Prof. M. Maczka, Prof. J.H. Ko, Prof. O. Yamamuro, Prof. H. Anwar, and Dr. Y. Matsuda for their collaboration and fruitful discussions. The author is also thankful to M. Kawashima, Y. Fukawa, K. Kaneda, S. Aramomi, and T. Sunaoshi for the experiments.

Author details

Seiji Kojima
Division of Materials Science, University of Tsukuba, Tsukuba, Japan

*Address all correspondence to: kojima@ims.tsukuba.ac.jp

IntechOpen

© 2022 The Author(s). Licensee IntechOpen. This chapter is distributed under the terms of the Creative Commons Attribution License (<http://creativecommons.org/licenses/by/3.0>), which permits unrestricted use, distribution, and reproduction in any medium, provided the original work is properly cited. 

References

- [1] Kauzmann W. The nature of the glassy state and the behavior of liquids at low temperatures. *Chemical Reviews*. 1948;**43**:219-256. DOI: 10.1021/cr60135a002
- [2] Kojima S. Anniversary of Brillouin scattering: Impact on materials science. *Materials*. 2022;**15**:3518. DOI: 10.3390/ma15103518
- [3] Vogel DH. Das Temperaturabhaengigkeitsgesetz der Viskositaet von Fluessigkeiten. *Physikalische Zeitschrift*. 1921;**22**: 645-646
- [4] Fulcher GS. Analysis of recent measurements of the viscosity of glasses. *Journal of the American Ceramic Society*. 1925;**8**:339-355. DOI: 10.1111/j.1151-2916.1925.tb16731.x
- [5] Franosch T, Götze W, Mayr MR, Singh AP. Evolution of structural relaxation spectra of glycerol within the gigahertz band. *Physical Review E*. 1997;**55**:3183-3190. DOI: 10.1103/PhysRevE.55.3183
- [6] Polge C, Smith A, Parkes A. Revival of spermatozoa after vitrification and dehydration. *Nature*. 1949;**164**:666. DOI: 10.1038/164666a0
- [7] Kojima S. Anomalous behaviour of the O-H stretching vibrational mode in the liquid-glass transition of glycerol. *Journal of Molecular Structure*. 1993;**294**:193-195. DOI: 10.1016/0022-2860(93)80347-X
- [8] Lunkenheimer P, Loidl A. Dielectric spectroscopy of glass-forming materials: α -relaxation and excess wing. *Chemical Physics*. 2002;**284**: 205-219. DOI: 10.1016/S0301-0104(02)00549-9
- [9] Kojima S. Low-frequency raman investigation of the liquid-glass transition in glycerol. *Physical Review B*. 1993;**47**:2924-2927. DOI: 10.1103/PhysRevB.47.2924
- [10] Ahart M, Ahiati D, Hemly R, Kojima S. The Boson peak of glassy glycerol under high pressure. *Journal of Physical and Chemical Part B*. 2017;**121**: 6667-6672. DOI: 10.1021/acs.jpcc.7b01993
- [11] Fajans K, Barber SW. Properties and structures of vitreous and crystalline boron oxide. *Journal of the American Chemical Society*. 1952;**74**:2761-2768. DOI: 10.1021/ja01131a019
- [12] Krogh-Moe J. The structure of vitreous and liquid boron oxide. *Journal of Non-Crystalline Solids*. 1969;**1**: 269-284. DOI: 10.1016/0022-3093(69)90025-8
- [13] Bengisu M. Borate glasses for scientific and industrial applications: A review. *Journal of Material Science*. 2016;**51**:2199-2242. DOI: 10.1007/s10853-015-9537-4
- [14] Shelby JE. Thermal expansion of alkali borate glasses. *Journal of American Ceramic Society*. 1983;**66**: 225-227. DOI: 10.1111/j.1151-2916.1983.tb10023.x
- [15] Kojima S, Kodama M. Velocity of sound in and elastic properties of alkali metal borate glasses. *Physical and Chemical Glasses*. 2014;**55**:1-12
- [16] Kodama M, Kojima S. Velocity of sound and elastic properties of Li₂O-B₂O₃ glasses. *Journal of Applied Physics*. 1995;**34**:2570-2574. DOI: 10.1143/JJAP.34.2570

- [17] Wright AC. Borate structures: Crystalline and vitreous. *Physics and Chemistry of Glasses: European Journal of Glass Science and Technology, Part B*. 2010;**51**:1-39
- [18] Greaves GN, Greer AL, Lakes RS, Rouxel T. Poisson's ratio and modern materials. *Nature Materials*. 2011;**10**: 823-837. DOI: 10.1038/NMAT3134
- [19] Zeller RC, Pohl RO. Thermal conductivity and specific heat of non-crystalline solids. *Physical Review B*. 1971;**4**:2029-2040. DOI: 10.1103/PhysRevB.4.2029
- [20] Nakayama T. Boson peak and terahertz frequency dynamics of vitreous silica. *Reports on Progress in Physics*. 2002;**65**:1195-1242. DOI: 10.1088/0034-4885/65/8/203
- [21] Ioffe AF, Regel AR. Non-crystalline, amorphous, and liquid electronic semiconductors. *Progress in Semiconductors*. 1960;**4**:237-291
- [22] Elliott SR. A unified model for the low-energy vibrational behaviour of amorphous solids. *Europhysics Letters*. 1992;**19**:201-206. DOI: 10.1209/0295-5075/19/3/009
- [23] Schirmacher W. Thermal conductivity of glassy materials and the 'boson peak'. *Europhysics Letters*. 2006;**73**:892-898. DOI: 10.1209/epl/i2005-10471-9
- [24] Leonforte F, Tanguy A, Wittmer JP, Barrat JL. Inhomogeneous elastic response of silica glass. *Physical Review Letters*. 2006;**97**:055501. DOI: 10.1103/PhysRevLett.97.055501
- [25] Galperin YM, Karpov VG, Kozub VI. Localized states in glasses. *Advances in Physics*. 1989;**38**:669-737. DOI: 10.1080/00018738900101162
- [26] Buchenau U, Galperin YM, Gurevich VL, Parshin DA, Ramos MA, Schober HR. Interaction of soft modes and sound waves in glasses. *Physical Review B*. 1992;**46**:2798-2808. DOI: 10.1103/PhysRevB.46.2798
- [27] Duval E, Garsia N, Boukenter A, Serughetti J. Correlation effects on Raman scattering from low-energy vibrational modes in fractal and disordered systems. I. Theory. *Journal of Physical Chemistry*. 1993;**99**: 2040-2045. DOI: 10.1063/1.465267
- [28] Götze W, Mayr M. R; Evolution of vibrational excitations in glassy systems. *Physical Review E*. 2000;**61**:587-606. DOI: 10.1103/PhysRevE.61.587
- [29] Chumakov AI et al. Equivalence of the boson peak in glasses to the transverse acoustic van Hove singularity in crystals. *Physical Review Letters*. 2011;**106**:225501. DOI: 10.1103/PhysRevLett.106.225501
- [30] Grigera TS, Martn-Mayor V, Parisi G, Verrocchio P. Phonon interpretation of the 'boson peak' in supercooled liquids. *Nature*. 2003;**422**: 289-292. DOI: 10.1038/nature01475
- [31] Lubchenko V, Wolynes PG. Theory of structural glasses and supercooled liquids. *Annual Review of Physical Chemistry*. 2007;**58**:235-266. DOI: 10.1146/annurev.physchem.58.032806.104653
- [32] Baggioli M, Zaccane A. Universal origin of boson peak vibrational anomalies in ordered crystals and in amorphous materials. *Physical Review Letters*. 2019;**122**:145501. DOI: 10.1103/PhysRevLett.122.145501
- [33] Hu YC, Tanaka H. Origin of the boson peak in amorphous solids. *Nature*

Physics. 2022;**8**:669-677. DOI: 10.1038/s41567-022-01628-6

[34] Kojima S, Novikov NV, Kodama M. Fast relaxation, boson peak and anharmonicity in lithium borate glass. *The Journal of Chemical Physics*. 2000; **113**:6344-6350. DOI: 10.1063/1.1309530

[35] Kojima S, Kawaji H. Low-temperature heat capacity of alkali metal borate glass. *Journal of Thermal Analysis and Calorimetry*. 2019;**135**:2759-2764. DOI: 10.1007/s10973-018-7590-3

[36] Kojima S, Novikov VN, Kofu M, Yamamuro O. Neutron scattering studies of static and dynamic correlation lengths in alkali metal borate glasses. *Journal of Non-Crystalline Solids*. 2019;**518**:18-23. DOI: 10.1016/j.jnoncrysol.2019.05.005

[37] Carini G, Gilioli E, Tripodo G, Vasi C. Structural changes and elastic characteristics of permanently densified vitreous B₂O₃. *Physical Review B*. 2011; **84**:024207. DOI: 10.1103/PhysRevB.84.024207

[38] Kojima S, Novikov VN, Kofu M, Yamamuro O. Nanometric fluctuations of sound velocity in alkali borate glasses and fragility of respective melts. *Physica Status Solidi B*. 2020;**257**:2000073. DOI: 10.1002/pssb.202000073

[39] White GK, Collocott SJ, Cook JS. Thermal expansion and heat capacity of vitreous B₂O₃. *Physical Review B*. 1984; **29**:4778-4781. DOI: 10.1103/PhysRevB.29.4778

[40] Shintani H, Tanaka H. Universal link between the boson peak and transverse phonons in glass. *Nature Materials*. 2008;**7**:870-877. DOI: 10.1038/nmat2293

[41] Lucovsky G, Galeener FL. Intermediate range order in amorphous solids. *Journal of Non-Crystalline Solids*.

1980;**35-36**:1209-1214. DOI: 10.1016/0022-3093(80)90362-2

[42] Greaves GN, Sen S. Inorganic glasses, glass-forming liquids and amorphizing solids. *Advances in Physics*. 2007;**56**:1-166. DOI: 10.1080/00018730601147426

[43] Salmon PS. Real space manifestation of the first sharp diffraction peak in the structure factor of liquid and glassy materials. *Proceedings of the Royal Society of London A*. 1994;**445**:351-365. DOI: 10.1098/rspa.1994.0065

[44] Zaug JM, Soper AK, Clark SM. Pressure-dependent structures of amorphous red phosphorus and the origin of the first sharp diffraction peaks. *Nature Materials*. 2008;**7**:890-899. DOI: 10.1038/nmat2290

[45] Sokolov AP, Kisliuk A, Soltwisch M, Quitmann D. Medium-range order in glasses: Comparison of Raman and diffraction measurements. *Physical Review Letters*. 1992;**69**:1540-1543. DOI: 10.1103/PhysRevLett.69.1540